Solar Phys (2011) 269: 129–140
DOI 10.1007/s11207-010-9686-1

Solar Activity Cycle in Solar-wind Sources and Flows

N.A. Lotova · K.V. Vladimirskii · V.N. Obridko

Received: 25 November 2009 / Accepted: 24 November 2010 / Published online: 31 December 2010

Abstract Experiments based on multi-source radio occultation measurements of the circumsolar plasma at $R \sim 4.0 - 70R_S$ were carried out during 1997–2008 to locate the inner boundary of the solar-wind transonic transition region, R_{in}. The data obtained were used to correlate the solar-wind stream structure and magnetic fields on the source surface ($R = 2.5R_S$) in the solar corona. The method of the investigation is based on the analysis of the dependence $R_{in} = F(|B_R|)$ in the correlation diagrams, where R_{in} is the inner boundary of the solar-wind transition region and $|B_R|$ is the intensity of the magnetic field at the source surface. On such diagrams, the solar wind is resolved into discrete branches, streams of different types. The analysis of the stream types using a continuous series of data from 1997 to 2008 allowed us to propose a physical criterion for delimiting the epochs in the current activity cycle.

Keywords Solar cycle · Solar magnetic fields · Solar wind

1. Introduction

The interest to study the solar wind and its sources has increased in recent years because of an unexpected anomaly, the extremely long minimum of cycle 23. In this context, we would like to mention a number of publications dealing with this problem that are associated with our present work (Veselovsky, 2009a, 2009b; Dmitriev, Suvorova, and Veselovsky, 2009; Efimov *et al.*, 2008; Manoharan, 2010). The sequence of phases in a solar cycle has lately become the subject of close examination, since the length of the minimum is difficult to determine. The question arises whether the current minimum is abnor-

N.A. Lotova (✉) · V.N. Obridko
Pushkov Institute of Terrestrial Magnetism, Ionosphere, and Radio-wave Propagation RAS, Troitsk, Russia
e-mail: nlotova2009@rambler.ru

K.V. Vladimirskii
Lebedev Physical Institute RAS, Moscow, Russia

mally long or, in other words, whether we are witnessing a failure of the solar periodicity. The solar periodicity has been investigated for about 160 years (Bumba and Kleczek, 1976; Vitinsky, Kopecky, and Kuklin, 1986). The phases of the solar cycle are determined conventionally from the Wolf number values R_Z (Ishkov, 2001). However, this is not universal. In particular, it is useless in the cycles in which (like the present one) the rate of rise and decline of activity is lower than in the majority of the previous cycles. The Wolf numbers, recorded for a long time, are of great scientific value as a source of straightforward information on solar activity (Ishkov, 2001) (www.dxlc.com/solar/solarcycle.html). Usually, the study of the duration of the cycle phases from the Wolf number series, $R_Z(t)$, is based on the analysis of the local fields alone.) In this work, we have used a different approach, which includes data on the total intensity of the global coronal magnetic field $I_{Br}(t)$ (Obridko and Shelting, 1992) and the solar-wind stream structure (Lotova *et al.*, 2002). This allowed us to propose a reliable physical criterion for identifying the cycle phases. The study below is based on three independent sets of data: radio scattering observations in circumsolar plasma at the radial distances $R \sim 4.0 - 70R_S$ obtained with the large radio telescopes DCR-1000 and RT-22 of the Pushchino Radio Astronomical Observatory, the configuration and intensity of the coronal magnetic field calculated from Zeeman observations at the John Wilcox Solar Observatory (Stanford, USA) [http://quake.stenford.edu//wso.html], and white-light images of the solar corona obtained with the *Large Angle and Spectrometric Coronagraph* (LASCO) on board the *Solar and Heliospheric Observatory* (SOHO) [http://sohowww.nascom.nasa.gov].

2. Particular Features of the Experiments Based on Multi-source Radio Occultation Measurements of the Circumsolar Plasma

Ground-based radio astronomic studies of interplanetary plasma and solar wind are traditionally carried out using compact, extragalactic radio sources, quasars (the so-called radio occultation method). Due to the annual rotation of the Earth, these sources are observed to alternatively approach and move away from the Sun. As they approach the Sun, their emission scatters on electron density inhomogeneities in interplanetary plasmas, thus increasing the apparent angular dimension of the source observed at Earth. This dimension, $2\theta(R)$, is determined by the radio-wave scattering cone with the scattering angle $\theta(R)$. The radio occultation method was first proposed by Vitkevich (1951, 1955) for the study of circumsolar plasma in the strong wave scattering regime when the phase incursion in the medium due to irregularities is $(\overline{\Delta S^2})^{\frac{1}{2}} \gg 1$. The strong wave scattering results in an increase of the "apparent" angular dimension of the source. The radio occultation method was initially used to study the interplanetary medium at a radial distance from the Sun R, with $R \approx 16R_S$. The further development of the method involved the study of farther regions and going to the weak-scattering regime $(\overline{\Delta S^2})^{\frac{1}{2}} < 1$. The scintillation of the occultation sources is studied in the weak-scattering regime where their principal characteristic, the scintillation index, is $m(R) < 1$:

$$m^2(R) = \frac{\overline{I^2} - (I)^2}{(\overline{I})^2}, \tag{1}$$

where I is the intensity of the occultation source.

The theory of radio scattering in randomly inhomogeneous media determines the relationship between the scattering angle $\theta(R)$ and scintillation index $m(R)$, on the one hand,

and the parameters of the scattering medium, on the other (Salpeter, 1967; Cohen, 1969; Hewish, 1971; Prokhorov *et al.*, 1974, 1975). In the simplest case of wave scattering on a thin phase screen with the effective scale of inhomogeneities a_{eff} and phase incursion $\overline{\Delta S^2}$, the relation between the scatter characteristics under discussion and the parameters of the medium has the form:

$$\theta = \frac{\lambda(\overline{\Delta S^2})^{\frac{1}{2}}}{2\pi a_{\text{eff}}} = \frac{\lambda \cdot \Delta S}{2\pi a_{\text{eff}}}, \tag{2}$$

$$m = \sqrt{2}\left(\overline{\Delta S^2}\right)^{\frac{1}{2}} = \sqrt{2}\lambda r_{\text{e}} L^{\frac{1}{2}} \cdot \Delta N_{\text{e}} a_{\text{eff}}^{\frac{1}{2}}, \tag{3}$$

where L is the effective scattering slab thickness, r_{e} is the electron radius ($r_{\text{e}} = 2.8 \times 10^{-18}$ km), λ is the received radio wavelength, and ΔN_{e} is the r.m.s. fluctuation of electron density. Equations (1) to (3) show that the scattering characteristics under examination, the angular dimension of the occultation source $2\theta(R)$ determined by the scattering cone and the scintillation index $m(R)$, are associated with the strong- and weak-scattering regimes, respectively; but their dependence on R is determined by the same parameter $\Delta N_{\text{e}}(R)$, which has the same radial dependence in the two cases.

Two different modifications of the radio occultation method were used in our experiments. One is used to study the radial dependence of the radio-wave scattering angle $2\theta(R)$ from quasar observations under strong-scattering conditions. In the other, the maser sources of the water vapor line $\lambda = 1.35$ cm were used for the first time as the occultation sources to study the radial dependence of the scintillation index $m(R)$ in the weak scattering mode (Lotova, Blums, and Vladimirskii, 1985; Lotova *et al.*, 2002). These modifications of the method could be combined after the solar-wind transonic transition region had been determined (Lotova, 1992). In the transition region, the subsonic flow gives way to the supersonic one due to the appearance of certain structural features in the radial profile $2\theta(R)$ and the scintillation index $m(R)$. Both functions were found to have similar shapes (Lotova, 1992; Lotova and Korelov, 1992; Lotova *et al.*, 2004). Thus, the structural features of the transition region make it possible to localize its inner R_{in} and outer R_{out} boundaries by the radial dependence of both the scattering angle $2\theta(R)$ and the scintillation index $m(R)$. The combination of two modifications of the radio occultation method and accumulation of a vast statistical database on the occultation sources allowed us to design experiments based on multi-source scintillation measurements of the circumsolar plasma. The quasar observations are carried out with the DKR-1000 radio telescope in the frequency range $\nu = 110.5 - 111$ MHz at the wavelength $\lambda \approx 2.9$ m. The maser sources of the water vapor line ($\lambda = 1.35$ cm) are observed with the RT-22 radio telescope at the working frequency $\nu = 22.2$ GHz with the use of a 426-channel spectrograph having a channel width $\Delta\nu = 6$ kHz. Three channels (the central and two lateral ones) are used independently in observations. Continuous annual observations cover the period 1997 – 2008. Figure 1 illustrates the radial dependence of the scattering angle $2\theta(R)$ as inferred from observations of the sources 3C215 (symbol △) and 3C225 (symbol ○) in 2001 (a) and the sources 3C133 (symbol ○), 3C154 (symbol △), 3C162 (symbol □), and 3C172 (symbol ▽) in 1991 (b). The open symbols correspond to the eastern heliosphere (E) and the filled ones, to the western heliosphere (W). The transition region appears here as an extensive zone of enhanced scattering compared to the subsonic region with its typical asymptotic dependence $2\theta(R) = CR^{-1.6}$. An important structural feature is the precursor of the transition region, a narrow zone of sharply reduced scattering, which precedes the extensive zone of enhanced scattering. The decrease of the scattering is

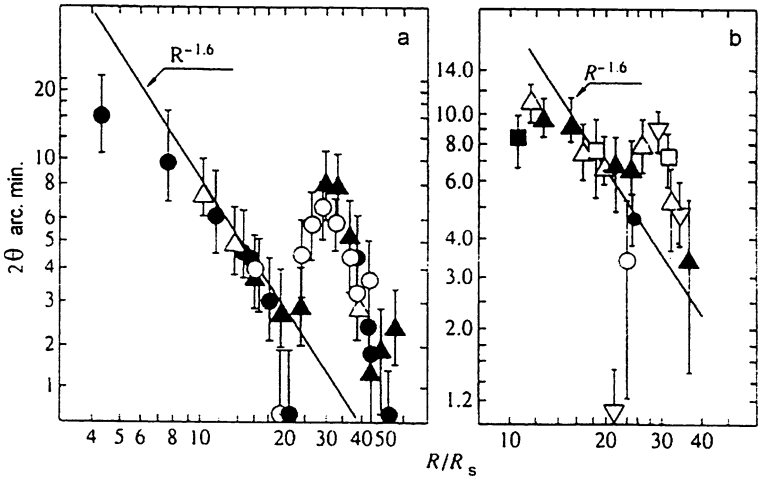

Figure 1 Radial dependence of the scattering angle $2\theta(R)$ as inferred from observations of the sources in 2001 (a) and 1991 (b).

a real phenomenon. It significantly exceeds the order of magnitude of the possible measurement errors. A small width of the precursor region allows us to use it as the inner boundary of the transition region R_{in} (Lotova, Vladimirskii, and Korelov, 1997).

3. Magnetic Fields in the Solar Corona

The structure and intensity of the coronal magnetic field in the source region were derived by solving the field equation in the region $R_S \leq R \leq 2.5R_S$. Calculations were performed under a potential approximation by the method developed at the *J. Wilcox Solar Observatory* (WSO) (Hoeksema, Wilcox, and Scherer, 1982) and at the *Institute of Terrestrial Magnetism, Ionosphere, and Radio Wave Propagation of the Russian Academy of Sciences* (IZMIRAN) (Obridko and Shelting, 1992). It is assumed that, up to a certain height, the field behaves like a field in the vacuum and is described by the current-free model. Above this boundary, called the source surface, and farther in the heliosphere, the field, on the contrary, is fully controlled by the solar wind. Right on the source surface, the field is strictly radial. Such a simple model gives the field at the Earth orbit, which agrees in magnitude and direction with that measured at the spacecraft. In this model, the problem is reduced to the solution of the Laplace equations in spherical coordinates with two boundary conditions. As the latter, we used WSO measurements on the solar surface, the sphere of radius $R = R_S$ (http://quake.stanford.edu//wso.html). The field on the source surface is radial and has a zero potential. As a result of the calculations, we obtained the absolute values of the radial component of the source surface field $|B_R|$ fitted in time and angular coordinates to R_{in} observations and the magnetic field structure in the solar corona. Since the solar-wind streams at $10 - 40R_S$ do not deviate significantly from the radial direction, the time and angular coordinates of radio observations were directly extended to the solar-wind source region, a sphere of radius $2.5R_S$, where the acceleration of solar-wind streams is believed to start. Thus, we had a unique opportunity to compare the data on plasma acceleration and speeds with magnetization of streams in the source region (Lotova *et al.*, 2002, 2004).

Besides that, we explored the type of field lines on the source surface to establish the conditions of penetration of the frozen-in magnetic field to the solar-wind streams. Below, we study the correlation between $R_{\rm in}$ and $|B_{\rm R}|$ in order to reveal the cause-and-effect relations in the solar-wind acceleration mechanism. The conclusions obtained are corroborated to a large extent by optical observations of the stream structure in the white-light corona and by the earlier independent comparison of *Ulysses* measurements of the solar-wind speed with our experimental values of $R_{\rm in}$ (Lotova *et al.*, 2002). The correlation diagrams for $R_{\rm in} = F(|B_{\rm R}|)$ and $V = F(|B_{\rm R}|)$ are plotted for two different phases of solar activity (1991 and 1995). Their analysis has shown that the stream types in both diagrams coincide.

4. Application of the Correlation Method to Analyze the Types and Structure of Solar-wind Streams

The diagnostics of the solar-wind streams is based on the study of correlation diagrams of the relation

$$R_{\rm in} = F\big(|B_{\rm R}|\big), \tag{4}$$

where $R_{\rm in}$ is the position of the inner boundary of the solar-wind transonic transition region, and $|B_{\rm R}|$ is the magnetic field intensity on the source surface in the corona ($R \sim 2.5R_{\rm S}$) (Lotova *et al.*, 2004). The correlation dependence $R_{\rm in} = F(|B_{\rm R}|)$ breaks up into several independent branches, corresponding to types of solar-wind stream. Such diagrams, based on the results of multi-source scintillation measurements of the circumsolar plasma during 1997 – 2008, are represented in Figure 2. As seen from the diagrams, the solar wind consists of discrete branches, streams of different types. The analysis of each branch in correlation with the calculated magnetic field has shown that the type of the stream depends on the field structure in the corona. Besides, the streams of different types were compared with the SOHO/LASCO C2 and C3 images (Lotova *et al.*, 2002, 2004) and were related to the particular configurations of the white-light corona. The data obtained are represented in Table 1. The columns show the stream type (fast/slow), the intensity of the source-surface magnetic field $|B_{\rm R}|$ (strong/weak), magnetic field configuration in the corona (open, closed, or mixed), and the structure of the white-light corona. The last column contains the symbols used to denote the stream types on the correlation diagrams in Figure 2. The table summarizes the data on the stream types and sources existing in the solar wind during an activity cycle. The data in the table were used to calculate the slope of the function $R_{\rm in} = F(|B_{\rm R}|)$ for the streamer-associated solar-wind component for different years (Figure 3). Figure 3 illustrates the cycle evolution of the streamer component. The data on the stream structure were used when discussing the behavior of the solar-wind parameters in different phases of the activity cycle.

The analysis of the set of correlation diagrams in Figure 2 and the tabulated data suggest that the stream structure of the solar wind is an extension of the structure of the coronal magnetic field and white-light corona to interplanetary space. It follows from the table that in the period 1997 – 2008, the solar wind might comprise as many as ten streams with different physical characteristics. Thus, the solar-wind structure is, obviously, much more complicated and diversified than it appeared before, when the solar wind was believed to consist of fast and slow streams with the intermediate velocity $V = 400$ km/s (Schwenn, 1990).

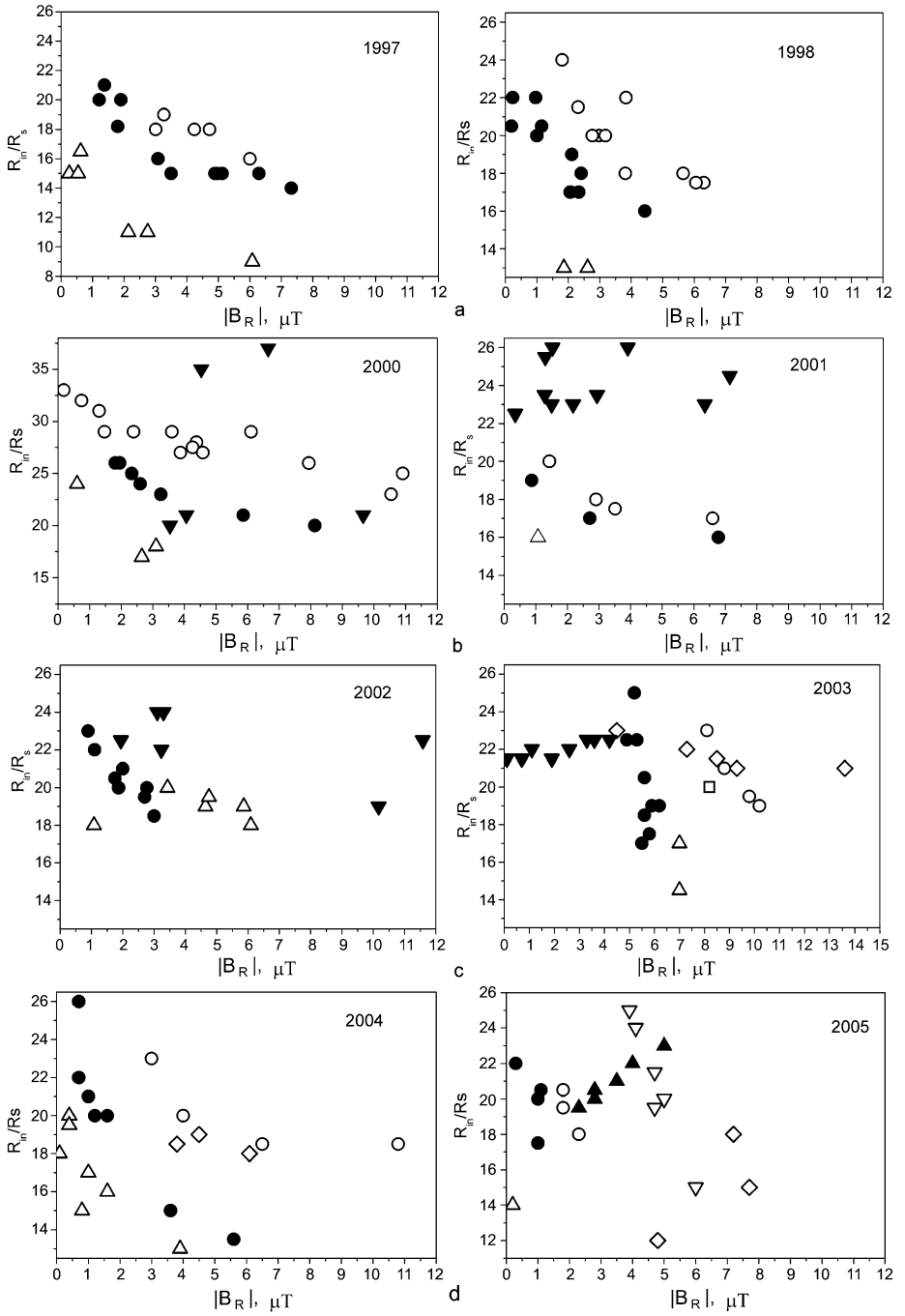

Figure 2 Correlation diagrams that illustrate the position of the inner boundary of the $R_{\rm in}$ of the transition region as a function of the field intensity in the corona $|B_{\rm R}|$ in the periods 1997 – 1998 (a), 2000 – 2001 (b), 2002 – 2003 (c), 2004 – 2005 (d), 2006 – 2007 (e), and 2008 (f). The solid line in Figure 2e (right-hand panel) represents the mean dependence $R_{\rm in} = F(|B_{\rm R}|)$ for the stream component associated with the large-scale polar coronal holes. Symbols denote different stream types listed in Table 1.

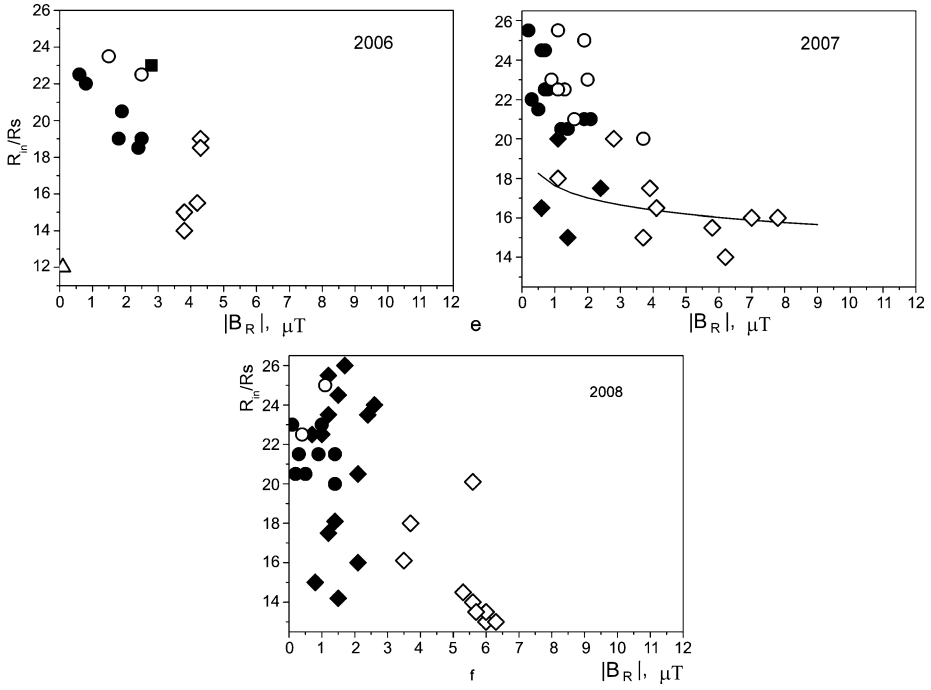

Figure 2 (*Continued*)

5. Wolf Number Cycle and General Intensity of the Global Coronal Magnetic Field

Up to now, the study of the solar periodicity was based mainly on the Wolf numbers, *i.e.*, the time variation of the local field alone was taken into account. In this approach, some convention is taken to separate the phases of the cycle following the variation of the Wolf number time series, $R_Z(t)$ (Ishkov, 2001). For example, the phase of the maximum is assumed to end when the maximum value $R_{Z\max}$ decreases by $\leq$15%. In Cycle 23, this corresponded to the period 2000 – 2002.

It would be interesting to study a more comprehensive characteristic of the coronal field, *i.e.*, the general intensity of the global magnetic field $I_{Br}(t)$. For this purpose, I_{Br} was calculated from the Stanford/WSO magnetic data [//quake.stanford.edu/wso/wso.html]. The calculation scheme and results are available in Hoeksema, Wilcox, and Scherer (1982), Obridko and Shelting (1992). In Figure 4, the time variation of the general intensity $I_{Br}(t)$ calculated for Cycle 23 is juxtaposed with the time dependence of R_Z [www.dxlc.com/solar/solcycle.html]. As seen from the figure, the two curves differ significantly both in the general shape and in the position of the main maximum (2003 for $I_{Br}(t)$ and 2000 for $R_Z(t)$). This results in different estimates of the duration of the phases of Cycle 23.

6. Cycle of Solar Activity in Solar-wind Streams

The set of correlation diagrams for 1997 – 2008 represented in Figure 2 illustrates the cycle evolution of the solar-wind streams. The figure reveals the particularities of the stream

Table 1 Structure of the solar-wind streams as inferred from the correlation diagrams $R_{in} = F(|B_R|)$, 1997 – 2008.

No.	Stream type	Magnetic field intensity $\|B_R\|$	Magnetic field structure	White-light corona structure	Symbols in Figure 2
1	Fast stream	Strong field	Open field lines	Large CH and polar CH	◇
2	Fast stream	Medium and weak field	Open field lines	Equatorial CH	◆
3	Fast stream	Weak field	Open structure in weak field	Side lobe of streamer	△
4	Very fast stream	Very weak field	Open field lines	Vicinity of the neutral line, probably, current sheet discontinuity	□
5	Slow stream	Medium and weak field	Closed field lines, loops, or mixed magnetic structure	Streamers	●
6	Slow stream	Weak field	Mixed structure	Weak diffuse glow: vicinity of streamer	○
7	Slow stream	Weak and medium field	Periphery of equatorial CH	Zone between streamer and dark region	▼
8	Slow stream	Weak field: ascending branch on the correlation diagram	Mixture of loop structures of different scales	Zone between streamer and CH	▲
9	Slow stream	Medium field	Extended magnetic loops	Loop connecting the vicinities of CH and curved HCS neutral line	■
10	Slow stream	Medium and strong field: descending branch on the correlation diagram	Mixed: loops and open field lines	Zone between streamer and CH	▽

structure in different phases of the activity cycle. In the rise phase (1997 – 1998), one can see a typical structure consisting of streams of three types. Later on (in 2000 – 2003), the correlation diagrams became much more complicated. A formerly unknown, uncorrelated component appeared (Figure 2b – c, symbol ◇). Here, the parameter R_{in} does not depend on the magnetic field intensity $|B_R|$. Another particularity of the period 2000 – 2003 is the increase of the slope of the relation $R_{in} = F(|B_R|)$ for the streamer component (Figure 3). As seen from Figure 3, the slope increased significantly in 2003 and began to decrease rapidly in 2004. In 2004 – 2005, the structure of the correlation diagram $R_{in} = F(|B_R|)$ changed dramatically (Figure 2d). The uncorrelated component vanished and two new, formerly unseen, components appeared. One of them, denoted with the symbol ▲, has a peculiar shape; the correlation $R_{in} = F(|B_R|)$ increases (and the stream speed decreases accordingly) with the increase of the field intensity (Lotova *et al.*, 1995). The period 2004 – 2005 is characterized by the appearance of numerous short-lived streams of the types not observed earlier (Figure 2d). Then, in 2006, another change occurred, the stream structure became plain and stable again consisting of three stream types and remained so till 2007 – 2008 (Figure 2e – f).

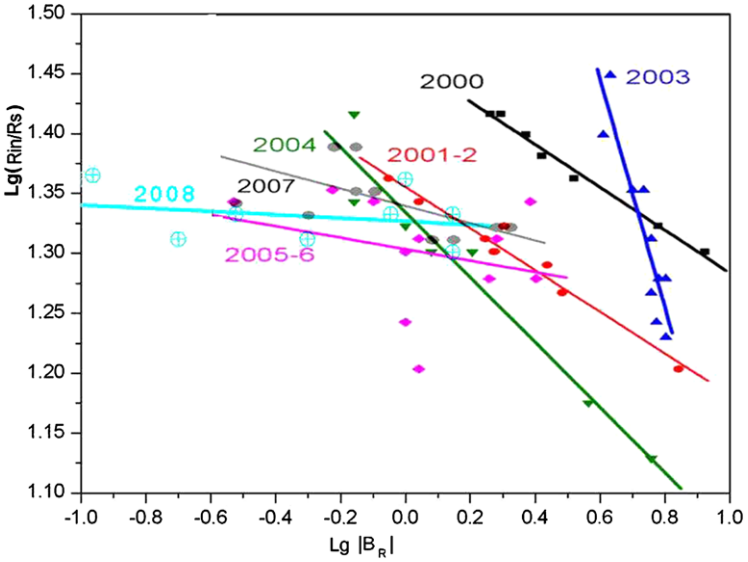

Figure 3 Cycle variation of the slope of $R_{\rm in}(|B_{\rm R}|)$ function for the streamer component. The convention is as follows: ■ – 2000, ● – 2001 – 2002, ▲ – 2003, ▼ – 2004, ◆ – 2005 – 2006, ● – 2007, ⊕ – 2008. Different colors are used for different fitting curves and corresponding symbols.

These regularities of the cycle evolution of the solar-wind streams allowed us to suggest a general physical criterion for the alternation of the cycle phases. The change of phases in the activity cycle occurs in the periods of radical evolution of the $R_{\rm in} = F(|B_{\rm R}|)$ correlation diagram. Thus, analyzing the set of correlation diagrams for 1997 – 2008, we can isolate the periods of reconstruction (2000, 2004, and 2006) and, accordingly, identify the phases of Cycle 23: the rise phase (1997 – 1999), maximum (2000 – 2003), declining phase (2004 – 2005), and beginning of the minimum (2006). Comparison of the phase boundaries obtained above with the time dependence of the Wolf numbers $R_{\rm Z}(t)$ and the general intensity of the global magnetic field $I_{\rm Br}$ leads us to the conclusion that the duration of the cycle phases is rather related to the latter (Figure 4).

7. Physical Criterion for the Alternation of Phases in the Activity Cycle

The $R_{\rm in} = F(|B_{\rm R}|)$ correlation diagrams for a long time interval 2000 – 2008 (Figures 2 and 3) show that reconstruction of the solar (coronal) magnetic field did not cease with the reversal of the dipole field in 2000 – 2002, but that it extended to different scales and components of the magnetic field. Figure 4 shows the time dependence of the general intensity of the global solar magnetic field $I_{\rm Br}(t)$, which illustrates this process, accompanied by variations in the $R_{\rm in} = F(|B_{\rm R}|)$ correlation diagrams represented in Figure 2. On the other hand, the widely used method of determining the phases of the solar activity cycle is based on the time dependence of the relative Wolf numbers $R_{\rm Z}(t)$; *i.e.*, it is assumed that the reconstruction of the solar magnetic field is determined by the evolution of the local fields (Ishkov, 2001). This explains the difference in the time variations $R_{\rm Z}(t)$ and $I_{\rm Br}(t)$ and in the duration of the solar maximum determined by two different methods: from the Wolf numbers $R_{\rm Z}(t)$ and from variation of the global solar magnetic field $I_{\rm Br}(t)$, which involves fields of

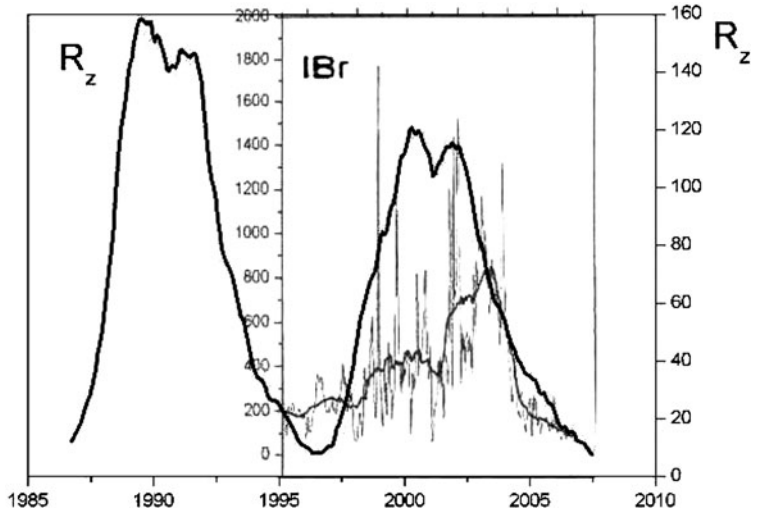

Figure 4 Time variation of the activity level as inferred from the Wolf numbers, $R_Z(t)$, and general intensity of the global solar magnetic field, $I_{\mathrm{Br}}(t)$.

different scales and structures (Figure 4). This means that we need a new physically consistent criterion for diagnostics of the solar cycle based on the study of the evolution of the solar-wind structure and time variations in the $R_{\mathrm{in}} = F(|B_{\mathrm{R}}|)$ correlation (Figure 2).

The correlation diagrams in Figure 2 and the data in Table 1 show that the evolution of the stream is associated with complex processes of permanent evolution of the existing stream components and types and with their changing number. On the whole, one can discriminate both stable and short-lived streams in the solar wind.

An aspect of special interest in the study of the solar-wind evolution is the correlation branch of the slow stream component associated with streamers (Figure 3), which is present all over the observation period. In Figure 3, this correlation branch is represented in logarithmic scale. The fitting curves are drawn using the least square method. As seen from Figure 3, the slope of the $R_{\mathrm{in}}(|B_{\mathrm{R}}|)$ function was increasing continuously in the years of maximum solar activity (2000 – 2002) and reached its greatest value in 2003. Then, in 2004, this process changed sharply. The slope of the stream component under consideration began to decrease reaching its minimum in 2006 – 2008. The time dependence of the slope of the streamer-associated slow component (inclination angle of the $R_{\mathrm{in}}(|B_{\mathrm{R}}|)$ function and its variation rate on the correlation diagram) agrees perfectly well with the time variation of the global solar magnetic field $I_{\mathrm{Br}}(t)$, which was increasing in 2000 – 2003, reached its maximum intensity in 2003, and, then, was decreasing during 2004 – 2008 (Figure 4).

At the time of the maximum of the Wolf number (2000 – 2002), the structure of the $R_{\mathrm{in}} = F(|B_{\mathrm{R}}|)$ correlation diagram changed, *i.e.*, a new, uncorrelated stream component appeared (Figure 2a – b, symbol $\diamondsuit$) and, simultaneously, the slope of the streamer-associated slow component increased gradually, as mentioned before (Figure 3). However, the $R_{\mathrm{in}} = F(|B_{\mathrm{R}}|)$ correlation diagram for 2003 (Figure 2b) shows that the aforementioned particularities of the diagrams for 2000 – 2002 persist also in 2003. This allows us to assert that the maximum of Cycle 23 lasted longer than previously thought and covered the interval 2000 – 2003. The end of the phase of maximum in 2003 was corroborated by subsequent observations. In fact, Figure 2d shows that in 2004, the $R_{\mathrm{in}} = F(|B_{\mathrm{R}}|)$ correlation diagram

changed fundamentally. The uncorrelated stream component disappeared and the slope of the slow component began to decrease. The change of the correlation diagram in 2004 is due to the appearance of a new type of streams (Figure 2d). In this period, the magnetic features of the previous phase (equatorial coronal holes) exist in the coronal magnetic field along with the new features of the coming phase (strongly elongated loops in a weak magnetic field). Let us compare these processes in the solar corona with the features on the correlation diagrams for 2004 – 2005, *i.e.*, magnetic loops of various scales: large elongated loops in a weak field, mixed loop structures (including high loops) in a medium-intensity field typical of 2005 (Figure 2c, symbol ▲), and, finally, elongated loops in a strong field (Figure 2c, symbol ▽). Thus, the phase of declining activity (2004 – 2005) is mainly characterized by the appearance of new features in the coronal magnetic field, *i.e.*, strongly elongated loops in a strong magnetic field. Simultaneously, the $R_{\rm in} = F(|B_{\rm R}|)$ correlation diagrams display new short-lived structures (Figure 2d) and the streamer-associated slope decrease of the slow component (symbol ●) .

The next fundamental change in the $R_{\rm in} = F(|B_{\rm R}|)$ correlation diagram occurred in 2006 (Figure 2e), when the diagram structure was simplified significantly, *i.e.*, only three stream components out of the six observed in 2005 persisted in 2006. The change of the coronal magnetic field in 2006 – 2008 to a simplified, more stable structure and a similar change in the solar-wind structure (Figure 2e) allow us to regard 2006 as the beginning of the solar minimum.

As seen from the evolution of the $R_{\rm in} = F(|B_{\rm R}|)$ correlation diagrams for 2000 – 2008, the beginning of each phase in the cycle of solar activity is accompanied by fundamental changes, *i.e.*, the disappearance of the streams characterizing the previous phase and the appearance of new stream types. Thus, the reconstruction of the correlation diagram can be used to establish the beginning of the cycle phase and ascertain the previous estimates of the duration of phases. According to the correlation diagrams for 2000 – 2008, the maximum of cycle 23 covered the period 2000 – 2003, the declining phase lasted from 2004 to 2005, and the minimum occurred in 2006.

The boundaries of the solar-cycle phases derived from the $R_{\rm in} = F(|B_{\rm R}|)$ correlation diagrams as described above can be compared with the estimates obtained from the time variation of the Wolf numbers $R_{\rm Z}(t)$ and global solar magnetic field intensity $I_{\rm Br}$ (Figure 4). The comparison allows us to suggest that evolution of the solar-wind streams and succession of epochs in the solar cycle are rather controlled by the intensity of the global magnetic field than by the local fields characterized by the Wolf numbers, as believed earlier.

8. Conclusion

New methods of investigation of the solar wind have significantly extended our knowledge of the solar-wind stream structure. Instead of the fast and slow components isolated earlier, we have recognized streams of ten different types. The type of the stream is determined by the structure of the magnetic field at the source. The relative contribution of the magnetic field at different scales changes significantly during an activity cycle. These changes are responsible for variations in the general intensity of the global magnetic field, $I_{\rm Br}(t)$, unlike the Wolf number variation, $R_{\rm Z}(t)$, which is based on the local magnetic field data alone. A physical criterion is proposed to determine the time limits of the phases in a solar cycle. It is based on the periods of fundamental reconstruction of the correlation diagram $R_{\rm in} = F(|B_{\rm R}|)$ when the streams of the previous phase disappear, being substituted by the streams of a new type.

The set of the $R_{\rm in} = F(|B_{\rm R}|)$ correlation diagrams for 1997 – 2008 allows us to isolate the periods of reconstruction (2000, 2004, and 2006) and, accordingly, to identify the phases of Cycle 23: the rise phase (1997 – 1999), maximum (2000 – 2003), declining phase (2004 – 2005), and the beginning of minimum (2006).

Acknowledgements The work was supported by the Russian Foundation for Basic Research, Projects no. 07-02-00115-a and no. 09-02-10002-k. We are grateful to the SOHO team and SWO for the data we have used in our study.

References

Bumba, V., Kleczek, J. (eds.): 1976, In: *Basic Mechanisms of Solar Activity*, *Proc. IAU Symp.* **71**, Reidel, Dordrecht. Russian translation: Obridko, V.N. (ed.): 1979, *Problemy solnechnoi aktivnosti*, Mir, Moscow.
Cohen, M.: 1969, *Annu. Rev. Astron. Astrophys.* **7**, 619.
Dmitriev, A.V., Suvorova, A.V., Veselovsky, I.S.: 2009, In: Johannson, H.E. (ed.) *Handbook on Solar Wind: Effects, Dynamics and Interactions*, Nova Science Publishers, Hauppauge, p. 81.
Efimov, A.I., Samoznaev, L.N., Bird, M.K., Chashei, I.V., Plettemeier, D.: 2008, *Adv. Space Res.* **42**, 117.
Hewish, A.: 1971, *Astrophys. J.* **163**, 645.
Hoeksema, J.T., Wilcox, J.M., Scherer, P.H.: 1982, *J. Geophys. Res.* **87**, 10331.
Ishkov, V.N.: 2001, *Zemlya i Vselennaya (Earth Universe)* **2**, 3 (in Russian).
Lotova, N.A.: 1992, In: Marsch, E., Schwenn, R. (eds.) *Solar Wind Seven*, *COSPAR Colloq. Ser.* **3**, Oxford, Pergamon, 217.
Lotova, N.A., Blums, D.F., Vladimirskii, K.V.: 1985, *Astron. Astrophys.* **150**, 266.
Lotova, N.A., Korelov, O.A.: 1992, In: Marsch, E., Schwenn, R. (eds.) *Solar Wind Seven*, *COSPAR Colloq. Ser.* **3**, Oxford, Pergamon, 221.
Lotova, N.A., Obridko, V.N., Vladimirskii, K.V., Bird, M.K., Janardhan, P.: 2002, *Solar Phys.* **205**, 149.
Lotova, N.A., Vladimirskii, K.V., Yurovskaya, I.Y., Korelov, O.A.: 1995, *Russ. Astron. J.* **72**, 757.
Lotova, N.A., Vladimirskii, K.V., Korelov, O.A.: 1997, *Solar Phys.* **172**, 225.
Lotova, N.A., Vladimirskii, K.V., Obridko, V.N., Subaev, I.A.: 2004, *Astron. Lett.* **30**, 387.
Manoharan, P.K.: 2010, *Solar and Stellar Variability: Impact on Earth and Planets*, *Proc. IAU Symp.* **264**, 356.
Obridko, V.N., Shelting, B.D.: 1992, *Solar Phys.* **137**, 167.
Prokhorov, A.M., Bunkin, F.V., Gochelashvili, K.S., Shishov, V.I.: 1974, *Usp. Fiz. Nauk* **114**(3), 415.
Prokhorov, A.M., Bunkin, F.V., Gochelashvili, K.S., Shishov, V.I.: 1975, *Proc. IEEE* **63**, 790.
Salpeter, E.E.: 1967, *Astrophys. J.* **147**, 433.
Schwenn, R.: 1990, In: Schwenn, R., Marsch, E. (eds.) *Physics of the Inner Heliosphere*, **1**, Springer, New York, 99.
Veselovsky, I.S.: 2009a, *Space Res. Today.* **174**, 67.
Veselovsky, I.S.: 2009b, *Geomagn. Aeron.* **49**(8), 1148.
Vitinsky, Yu.I., Kopecky, M., Kuklin, G.V.: 1986, *Statistics of Sunspot Generation Activity in the Sun*, Nauka, Moscow.
Vitkevich, V.V.: 1951, *Sov. Phys. (Dokl. RAN)* **77**(4), 585.
Vitkevich, V.V.: 1955, *Astron. Zh.* **32**(2), 106.